Evidence that deliberate marine cloud brightening can be more effective than previously thought

Ying Chen (y.chen.21@bham.ac.uk)
University of Birmingham https://orcid.org/0000-0002-0319-4950

Jim Haywood
University of Exeter https://orcid.org/0000-0002-2143-6634

Yu Wang
ETH Zurich, https://orcid.org/0000-0002-9480-3570

Florent Malavelle
Met Office

George Jordan
Met Office Hadley Centre https://orcid.org/0000-0002-3129-4983

Amy Peace
University of Exeter

Daniel Partridge
University of Exeter https://orcid.org/0000-0002-5970-901X

Nayeong Cho
NASA GSFC / UMBC https://orcid.org/0000-0001-6401-2391

Lazaros Oreopoulos
NASA-GSFC https://orcid.org/0000-0001-6061-6905

Steven Platnick
NASA GSFC

Daniel Grosvenor
Leeds University

Paul Field
Met Office/Univ. of Leeds

Richard Allan
University of Reading https://orcid.org/0000-0003-0264-9447

Ulrike Lohmann
ETH Zürich https://orcid.org/0000-0001-8885-3785

Article

Keywords:

Posted Date: September 22nd, 2023

DOI: https://doi.org/10.21203/rs.3.rs-3291831/v1

Abstract

With global warming currently standing at approximately + 1.2 ^{o}C, climate change is a pressing global issue. Marine cloud brightening (MCB) proposes injecting aerosols into marine clouds to enhance their reflectivity and thereby planetary albedo. However, because it is unclear how aerosols influence clouds, especially cloud cover, both climate projections and the effectiveness of MCB remain uncertain. Here, we use volcanic eruptions to quantify the aerosol fingerprint on tropical marine clouds. We observe a large enhancement in reflected sunlight, mainly due to an aerosol-induced increase in cloud cover. This observational evidence of a strong aerosol impact suggests that the Earth's climate is highly sensitive to external forcing mechanisms, but also that mitigation of global warming via MCB is more plausible than current climate models suggest. Our results suggest that the best efficacy for MCB practice is to seed clouds in humid and stable meteorological conditions.

Introduction

Aerosol-induced increases in liquid cloud opacity cool the Earth by enhancing reflection of sunlight back to space and could offset a large, yet poorly quantified, portion of greenhouse gas warming[1]. The climate impacts of aerosol-cloud interactions (ACI) have been widely debated in the past few decades and still constitute one of the largest uncertainties in the estimate of radiative forcing[1–3], impeding a better understanding of climate sensitivity[4] and the remaining carbon emission budget for avoiding overshoot the + 1.5 ^{o}C climate target[5,6]. However, as this target is in peril[4], proposals have emerged to help mitigate devastating climate impacts by conducting deliberate marine cloud brightening (MCB) to "buy some time"[7,8], whilst the global economy is decarbonizing. At regional scales, scientists are experimenting with MCB to save the Great Barrier Reef from the local warming of seawater[9]. However, the efficacy and potential side-effects of MCB are not well evaluated, due to an incomplete understanding of ACI.

The underlying principle of MCB is the ACI cooling effect, and the goal is to enhance the planetary albedo by seeding marine clouds with aerosols. The cooling effect of ACI originates from aerosols serving as cloud condensation nuclei (CCN), the seed of cloud droplets. Higher aerosol loadings typically lead to more but smaller cloud droplets, resulting in enhanced cloud albedo and thus more solar radiation reflection, a phenomenon known as the Twomey effect[10]. Smaller cloud droplets potentially slow down the collision-coalescence process and could delay precipitation, leading to a longer cloud lifetime and hence larger cloud cover and water content (lifetime effect)[11]. On the other hand, more but smaller cloud droplets could also enhance entrainment-evaporation from dry free troposphere air, possibly leading to a decrease of cloud coverage and albedo (entrainment effect)[12]. The ACI climate impact is determined by the net effect of the above processes, which are poorly constrained or represented in climate models[1,13,14] resulting in large uncertainties in the magnitude and even inconsistent in a positive or negative sign of efficacy when evaluating MCB using multi-model ensembles[14].

One reason for the slow progress in the development of realistic simulations of ACI in climate models is the lack of observational constraints[4,6]. Satellite observations of aerosol and clouds have been widely employed to study ACI using either small-scale natural experiments or large-scale climatological approaches. While both are useful, they do not provide sufficient constraints[6,13,15]. Small-scale natural experiments, such as ship-tracks and industrial plumes manifested as linear features of brighter clouds, are the most prominent pathway to study ACI because confounding meteorological co-variability can generally be ruled out, e.g.: ref.[5,16]. Large-scale climatological studies, e.g.: ref.[17,18], investigating spatiotemporal co-variability between aerosol and clouds, while more suitable for constraining large-scale global climate models [19] are often contaminated by the potential influence of meteorological co-variability on clouds[6,13]. Despite of these respective limitations, aggregating large observational ensemble of small-scale and large-scale satellite observations have resulted in convergence of ACI's impacts on cloud microphysical properties in recent studies[5,18]: a larger cloud droplet number concentration (N_d) reduces cloud droplet effective radius (r_{eff}) and brightens clouds with negligible change in cloud liquid water path (LWP). However, ACI's impact on cloud macro-physical properties, such as cloud cover, is persistently disputed, with disagreement of several orders of magnitude between observations and models[1,6,13,14]. This is because the large-scale nature of cloud macro-physical properties implies that small-scale approaches struggle[5], while traditional climatological large-scale approaches are hampered by confounding meteorological co-variability[6,13,20].

MCB would be most effective if cloud cover were to increase strongly[14,21], making urgent the task of improving how aerosol fingerprints on cloud cover are constrained and modelled. Large-scale degassing volcanic eruptions offer ideal natural experiments to investigate the overall impacts of ACI on climate[6,18,22] with implications for MCB. A recent study of ours developed a novel machine-learning approach to quantitatively disentangle aerosol fingerprints on clouds from the noise of meteorological co-variability and demonstrated its fidelity using a high-latitude degassing volcano in Iceland[6]. Building on this approach, here we disentangle the aerosol fingerprints on tropical marine convective clouds and further quantify its radiative cooling as an analogy to MCB, using four months of observations of volcanic eruptions in Hawaii (Fig. 1), each with distinct meteorological conditions. These unique natural experiments in the tropics not only provide invaluable constraints for improving climate models but also have great practical implications. While areas of stratocumulus frequently reach close to 100% cloud cover, the cloud fraction in areas of tropical oceanic shallow convective clouds are frequently much less than 50% – any MCB-induced change in the cloud fraction in these areas could have a disproportionally large cooling impact. This was one motivation behind the Geoengineering Model Intercomparison Project-6 (GeoMIP6) whose solar radiation management simulations (G4sea-salt) modelled the effectiveness of injecting sea-salt aerosols into the tropical marine boundary layer to offset a positive forcing (warming) of 2 W m^{-2}.[23]

The strong ACI cooling we find in this study due to the observed increase in cloud cover suggests that the observed global mean temperature change is a consequence of a small net radiative forcing[24], because

of warming forcing from greenhouse gases being counter-balanced to a large degree by ACI. This implies that a very high climate sensitivity is possible[4,17,24], something generally overlooked in climate models[25] but in line with recent observed paleoclimate evidence, as summarized in Hansen et al.[4] and references therein. Our study also suggests that the effectiveness of MCB may be more potent than that suggested by the current state-of-the-art climate models. This underscores the urgent need for additional well-designed studies into the efficacy and risks of MCB[26], perhaps a last resort in alleviating the increasing severity of climate impacts. We therefore call for improved ACI representation in climate models, especially with regard to cloud cover response.

Results

To quantify aerosol fingerprint on clouds and hence evaluate MCB, we build machine-learning surrogates of satellite observations to diagnose cloud properties and radiative fluxes for given meteorological conditions (see Methods). Using this approach, we can reproduce clouds under “normal” unperturbed conditions and compare to observations perturbed by volcanic eruptions. Surrogates are generated using 20 years of satellite observations of cloud properties, radiative energy fluxes, precipitation and co-located meteorological parameters, and are well validated against observations using advanced statistical approaches (Fig. 2, Supplementary Section S1 and Extended Data Fig. 1, see also details in Methods). Four months of degassing volcanic eruptions at Kilauea in Hawaii during June and July in 2008 and 2018 are investigated. The Hawaii-Kilauea volcanic outgassing events provide excellent natural experiments for assessing the effects of aerosol on clouds and climate due to the characteristics of the volcanic emissions and the pristine environment. These four experiments represent distinct meteorological conditions (Table 1 and Extended Data Fig. 2, see also Methods), with a tropical cloud regime spectrum of mainly oceanic shallow convective clouds representing a very different but MCB-relevant case compared to our previous high-latitude study of the Holuhraun eruption in Iceland (Extended Data Fig. 3). Almost all clouds in this studied region are likely to be precipitating, as suggested by $r_{eff} > 14$ μm (Extended Data Fig. 2)[17,27]. The June 2008 case is a balance of different meteorological conditions, with a wide range of lower-tropospheric stability (LTS) and relative humidity (RH). LTS is calculated as the difference in the potential temperature between 700 hPa and the surface[28], and LTS < 14 K indicates strongly unstable conditions[17]. Here, we analyse the RH at 850 hPa, as being representative for the layer between 700 hPa and the ocean surface. July 2008 is a special case with distinct bimodality of very dry conditions in the south and humid air in the north of the studied region (Fig. 3a). Natural experiments in 2018 represent humid conditions with more stable condition in June (nearly all LTS > 14 K) than in July.

Table 1
Description of meteorological conditions for each natural experiment case. The meteorological details are analyzed in Extended Data Fig. 2

Natural Experiments	Description
2008-06	Wide range of RH and LTS, including very unstable conditions (LTS < 14 K)
2008-07	Special case: dry-stable conditions in the southern part and humid-unstable conditions in the northern part of the studied region
2018-06	Humid environment with dominantly RH > 70%, very stable with nearly LTS > 14 K everywhere
2018-07	Very humid environment with dominantly RH > 75%, medium stability

We find that the volcanic aerosol leads to a significant Twomey effect, with N_d increasing by 26–28% and r_{eff} decreasing by 5–7%, on average over the region studied (Fig. 2, and Extended Data Fig. 4–7). This is consistent with many previous studies, e.g. ref.[5,17,18,22,27,29], of well-documented Twomey effect as an indicator of ACI. The LWP adjustment on the other hand has been more unclear overall, with both increases, decreases and no changes reported[5,6,16,18,27,30]; our observations indicate a statistically significant 4–6% decrease of the in-cloud LWP when aggregated over this large region. This is different from our previous high latitude study of the Holuhraun volcanic eruption[6], where LWP did not change for a different cloud regime under different meteorological conditions. The Holuhraun eruption occurred in a region where about 40% of the clouds are precipitating, while the Kilauea eruption occurred in a tropical region dominated by shallow oceanic convective clouds (Extended Data Fig. 3), 90% of which are likely to be precipitating (indicated by r_{eff} > 14 μm[17]). The decrease in LWP could be due to an increase of rainfall (Fig. 2), as clouds are still precipitating despite the reduction in r_{eff} and/or because of entrainment of dry air inducing cloud evaporation, as indicated by the dry southern part of the domain in July 2008 (Fig. 3a). The reduction of in-cloud LWP suppresses cloud brightening effect, also known as “buffering”[31].

However, we find a strong increase in cloud cover (also known as cloud fraction, CF) due to volcanic aerosol injection, enhancing the shortwave radiative cooling at the top of atmosphere (TOA) by about 4 W m^{-2}, 7.75 W m^{-2} and 14.7 W m^{-2} in June 2008, June 2018 and July 2018, respectively. July 2008 is the only exception without a statistically significant change in TOA cooling. A possible reason is the partial cancellation of the effects of cloud cover increase in the northern humid region and decrease in the southern dry region. We estimate the relative contributions to ACI shortwave cooling using Eq. (1) (see Methods), and find cooling from the Twomey effect (45% in the balanced and more generalized condition of June 2008; 13–16% in humid conditions in 2018), warming from LWP adjustment (-20% in June 2008; -10% to -5% in humid conditions) and cooling from cloud cover enhancement (75% in June 2008; 92–94% in humid conditions). Although June 2018 shows the strongest relative increase of cloud cover by + 54% (Fig. 2b, 1.53–0.99 = 54%), July 2018 shows a stronger enhanced TOA shortwave reflection by + 18%.

This is possible due to different meteorology, cloud regimes and solar zenith angles in these two months (Extended Data Fig. 2–3). A previous study of the Kilauea eruption using a climatological anomaly approach of satellite observations qualitatively identified the cloud cover increase in summer 2018 when the atmosphere was humid and the cloud cover response strong, but also reported a contrasting negative cloud cover response in summer 2008.[22] This indicates the critical influence of meteorological co-variability which our methodology removes to provide quantified ACI signals across four months in 2008 and 2018, that can serve as quantified constraints for global climate models.

We find a high susceptibility of cloud cover to changes in N_d ($dlnCF/dlnN_d = 0.38$) for the more generalized case of June 2008 (Fig. 2), consistent with our previous study of the Holuhraun natural experiment[6]. Extremely high cloud cover susceptibility ($dlnCF/dlnN_d > 1.0$) is found in humid conditions (in 2018 and in the northern humid region in July 2008); $dlnCF/dlnN_d$ can reach up to 1.6 in humid and stable conditions (June 2018, Fig. 2), which favours higher cloud cover[28,32]. This means that a 30% increase of N_d, which is the estimate of the averaged increase from pre-industrial to present-day conditions[13], could lead to a 10% relative increase in cloud cover overall (e.g. Holuhraun[6] and June 2008 cases with a mixture of meteorological conditions); and up to a 50% relative increase under humid and stable conditions, leading to much stronger TOA cooling (and weaker cooling under dry conditions which suppress cloud cover increases through more cloud top entrainment and cloud droplet evaporation).

Discussion

Recent research underlines the remarkable impacts of aerosols on clouds and climate change, and the fact that these strong impacts are potentially concealed when using traditional analysis approaches that suffer from biases associated with sampling, scale limitations and meteorological co-variability[16,19,20,33]. In this study of Kilauea natural experiments, we overcome the challenges of sampling small-scale episodes, and are able to quantify the significant aerosol fingerprints on clouds and climate forcing by investigating a large region (2500 km × 1500 km) and by ruling out the noise of meteorological co-variability using a long-term observation-based machine-learning approach (see Methods). The uncertainty in satellite retrievals over low-latitudes is expected to be relatively small compared to higher latitudes due to a smaller solar zenith angle[34,35]. In addition, random uncertainties in satellite retrievals are naturally cancelled out with averaging over a large region, and systematic uncertainties are minimized as well by comparing satellite observations against their machine-learning surrogates[6].

Our findings suggest that marine cloud brightening may be quite effective for alleviating climate warming, although it would likely materialize through an increase in cloud cover rather than brighter existing clouds, as the MCB terminology implies. Our results suggest that the best approach would be to seed clouds under humid and stable conditions (Fig. 4) where new clouds would form even if pre-existing clouds are sparse. Seeding clouds under dry conditions could lead to reduction of cloud cover and warming, opposing the intention to increase reflected solar radiation to space. This best practise would be particular effective in tropical oceans where incoming solar radiation is strong and background

environment is clean (i.e., clouds are more “pristine”), as demonstrated by the June 2018 case where cloud cover increased by 54% and resulted in a strong TOA cooling.

While effective, MCB can only be seen as a “pain killer”, since it does not address the cause of warming from anthropogenic greenhouse gases. Our results illustrate the high potential risk of unforeseen large “side-effects” of MCB, owing to the large uncertainty due to a poor understanding of aerosol-cloud interactions. This new finding of a large-scale strong cloud cover response taking place in different climate and cloud regimes, as demonstrated by the high-latitude Holuhraun[6] and tropical Kilauea eruption natural experiments, is however, not replicated by state-of-the-art global climate models[1,6,13,14,32]. It is paramount that we close current gaps in ACI knowledge in a fundamental way not only to advance our understanding of Earth climate system and its hydrological cycle, but also for a holistic evaluation of the benefits and risks of MCB.

Such a strong increase of large-scale cloud cover has remained undetected in many previous studies, e.g., ref.[5,16,18,19,36], and has been intensely debated in a few modelling and climatological studies[17,22,37,38]. The current theoretical understanding suggests that cloud cover increases via inhibition of precipitation[11], while our new findings demonstrate that cloud cover can increase even as rainfall strengthens (Fig. 2). We propose the following mechanism to explain this newly-observed phenomenon. As more aerosols activate, N_d increases, leading to the Twomey effect. For stratocumulus clouds embedded in an aerosol-abundant regime, this can inhibit precipitation and hence increase cloud lifetime. In an aerosol-limited and convective regime, the Twomey effect reduces r_{eff} but not sufficiently to efficiently slow down collision-coalescence, hence is not effective in inhibiting rainfall. Instead, when the atmosphere is humid, an increase of aerosols not only prolongs the lifetime of pre-existing precipitating clouds but also generates new ones, leading to more rainfall (Fig. 1b). Our case of tropical shallow convective clouds in a pristine marine environment[22], with $r_{eff} > 14$ μm and N_d mostly in the range of 15–35 cm^{-3} (Extended Data Fig. 1), is considered an aerosol-limited regime[39]. The mechanism that we are proposing would mean that new particle formation plays an even more critical role in Earth climate system than previously thought, especially in aerosol-limited environments (such as pre-industrial) where new particle formation is a major source of cloud condensation nuclei and where cloud cover is highly susceptible to increase in aerosol. This mechanism needs to be tested by further research, ideally by large eddy modelling of both the Holuhraun and Kileaua events to reproduce the different ACI mechanisms prevailing in different meteorology and cloud regimes. With advanced process-level understanding to inform the development of prognostic cloud cover schemes, a more detailed representation of subgrid-scale variability than diagnostic schemes currently used in most climate models[40,41], could serve as a plausible direction to improve ACI and hence predicted cloud feedbacks which remains the largest source of uncertainty in climate projections for decades.

This study sheds additional light on the understanding of aerosol fingerprints on clouds, especially with regard to cloud cover response. This is critical for more reliable climate projections, and underscores the

urgent need to have a sound theoretical foundation before implementing global warming mitigation strategies, such as MCB, which may have unintended consequences[26].

Methods

Natural experiment of Kilauea volcano on Hawaii

Kilauea is a volcano on the island of Hawaii (19° 34’ N, 155° 30’ W), situated in the middle of the North Pacific Ocean thousands of km away from major anthropogenic emission sources. The marine environment surrounding Kilauea is very close to pristine[22,42] with concentrations of cloud condensation nuclei thought to be close to those of the pre-industrial conditions in summer time[43]. Therefore, the degassing eruptions of Kilauea offer excellent natural experiments to investigate how clouds respond to aerosol perturbation (i.e., aerosol-cloud interactions, ACI).

Kilauea was strongly active in June-August 2008 and May-July 2018[22], with SO_2 emission peaks over 10 kiloton per day in 2008[44] and over 100 kiloton per day in 2018[45]. The volcanic SO_2 plumes (Fig. 1) and the subsequent formed particulate sulfate via SO_2 oxidation were efficiently dispersed over the downwind marine region as far as 6000 km[42]. The plumes reached up to 1200–2500 m height in 2008, and about two to eight km height in 2018[45]. The ocean water entry of eastern rift zone in 2018 eruptions introduced water vapor into the plume and humidified the lower troposphere[22,45], providing excellent natural experiments in contrasting humid conditions. In this study, we chose the summer months of June and July, which are common to both volcanic periods in 2008 and 2018 and allow us to distinguish aerosol fingerprints on shallow convective marine clouds in the tropics under different meteorological conditions. The natural experiment study focused on a downwind region (12 ^{o}N ~ 25 ^{o}N, 160 ^{o}W ~ 180 ^{o}W) strongly impacted by volcanic plumes (Fig. 1), see also the Fig. 2 in ref.[22].

Normal conditions of clouds and precipitation from machine-learning

Following our recent study[6], a one hundred trees random forest machine-learning (ML) algorithm is adopted to train a surrogate for the Moderate Resolution Imaging Spectroradiometer (MODIS). Random forest is adopted because of its great capability to avoid overfitting and handle high-dimensional feature spaces with a relatively small sample size. A ML surrogate is designed to diagnose cloud properties, which are unperturbed by volcanic aerosols, based on 114 meteorological parameters from the surface up to the 550 hPa level under which virtually all low-level liquid clouds occur. A full list of meteorological parameters is provided in our previous work, and details of the random forest approach are also given in ref.[6]. The training of the ML surrogate is performed for June and July separately and is supervised by MODIS observations of cloud properties (N_d, r_{eff}, LWP, and CF) under normal conditions during 2001–2020 by excluding the volcanic years 2008 and 2018. The ML surrogate is therefore able to predict unperturbed cloud conditions and enables like-with-like comparisons against volcanic perturbed clouds

observed by MODIS in 2008 and 2018. This approach has been demonstrated to work excellently in discerning the large-scale aerosol fingerprint on clouds from the noise of meteorology co-variability[6]. To distinguish aerosol fingerprint on precipitation, this ML-surrogate approach is also applied to the Global Precipitation Climatology Project (GPCP) dataset[46].

The ERA5 meteorological reanalysis from the European Centre for Medium-Range Weather Forecasts (ECMWF) is used to provide the best estimate of the atmospheric state[47] for ML surrogate training. We take ERA5 monthly averages of meteorological conditions at $0.25^{o} \times 0.25^{o}$ horizontal resolution from the surface up to 550 hPa at 50 hPa intervals, and aggregate them to MODIS and GPCP grid cells at the time of Aqua and Terra daytime overpasses. The ERA5 meteorology corresponding to Aqua and Terra overpassing time is used in this study. The top-10 most important meteorological variables for predicting CF in 2008 and 2018 are mostly lying within the variation range of the training dataset, indicating reliable ML training[6]. The only exception is the unprecedented dry condition (850 hPa RH < 50%) in the southern part of the studied region in July 2008 which lies outside the range of the training dataset. However, this exception is not expected to have a large influence on our cloud analysis, because the fraction of outliers is only about 10% of the total data points in July 2008. In addition, the extrapolation for these very dry conditions is performed in a regime where cloud response has levelled (Extended Data Fig. 8).

MODIS provides continuous satellite observations of clouds in June and July during 2003–2020 for Aqua and 2001–2020 for Terra. We use the latest MODIS Collection 6.1 Level-3 products, which has rectified retrieval biases in the previous Collection 5 and shows excellent consistency between Aqua and Terra[18]. The MODIS Level-3 monthly product is aggregated from Level-2 products with 1-km nadir resolution, and provides monthly-mean values of cloud optical thickness, cloud phase, cloud droplet effective radius (r_{eff}), in-cloud liquid water path (LWP), and cloud fraction (CF). The “cloud optical property CF” for liquid clouds[48] is used, because it is based on the pixel population with successful retrieval of cloud optical properties and is consistent with the other microphysical retrievals used in this study. Following ref.[49,50], we derived cloud droplet number concentrations (N_d) from daily Level-3 products of r_{eff} and cloud optical thickness and then aggregated the data to monthly mean values. The uncertainty in derived N_d is about 50% in general when averaging across a $1^{o} \times 1^{o}$ grid cell[34]. This uncertainty is expected to be much smaller in this study, because of a) lower uncertainty in the tropics compared to mid-latitudes[34], b) lower uncertainty in precipitating clouds[33] (> 90% in this study), and also c) extensive averaging over a 2500 km × 1500 km geographical region which greatly suppresses random errors.

GPCP combines datasets from rain gauge stations, sounding observations and various satellites to provide the best estimate of precipitation on a global scale[46]. The GPCP monthly accumulated rainfall with a $2.5^{o} \times 2.5^{o}$ horizontal resolution in June and July 2001–2020 (excluding 2008 and 2018) is used to supervise the ML training of the GPCP surrogate to represent rainfall under unperturbed normal conditions.

The performance of the ML surrogate in reproducing satellite observations under normal conditions (without the perturbation of volcanic aerosol) is demonstrated using the “leave-one-year-out” cross validation[51]. Here, one normal year is held for validation, the ML is trained based on the datasets of the other normal years, and the evaluation is performed once for each normal year in 2001–2020 (left panels of Extended Data Fig. 1). We further estimate the uncertainty of the ML surrogate using a more statistically robust bootstrapping Monte Carlo method. This method selects two out of 18 normal years (2001–2020 excluding 2008 and 2018) as the hold-years for validation in a bootstrapping way (uniform sampling with replacement), and trains ML based on the remaining normal years. This greatly enlarges the diversity of the sample pool, with 324 (18 × 18) different sample-variants in total, and therefore improves the robustness of the statistical analysis. We repeated this bootstrapping select-validation process for each ML surrogate for 648 times (twice the number of the total variants), to ensure the pool is efficiently sampled. The bootstrapping validation of ML surrogates are shown in the black boxplots in Fig. 2 and Fig. 3c-3d. The ratios between ML surrogate (without aerosol perturbation) and observations in volcanic years (MODIS or GPCP in 2008 or 2018, with aerosol perturbation) are shown in the red boxplots of Fig. 2 and Fig. 3c-3d. These red boxplots show the variability of the aerosol fingerprints on clouds. The significance of the statistical difference of cloud properties and precipitation between the perturbed and unperturbed conditions is tested by both the one-tail and two-tail Wilcoxon-Mann-Whitney test with p-values < 0.05 (significance > 95%).

Radiative forcing

We further use the above ML approach to train a surrogate to represent the unperturbed top-of-the-atmosphere (TOA) outgoing shortwave flux, which is observed by the CERES sensor on Terra and Aqua satellites[52]. This enables us to quantify the volcanic aerosol impact on the cooling effect of cloud. Following the above bootstrapping approach, the ML surrogate of CERES is validated, and the aerosol-induced change in cloud shortwave radiative forcing is quantified.

We estimate the contributions from the Twomey effect, LWP and CF adjustments to ACI-induced radiative cooling using the susceptibilities of r_{eff}, LWP and CF to aerosol-induced change in N_d. The ACI-induced total radiative cooling can be described as Eq. (1)[3,5,53], which is a modified version of Eq. (3) in ref.[6]. The relative contributions from the Twomey effect, LWP adjustments, and cloud cover adjustment are described in the Eq. (1) from left to right by the three terms in the square bracket.

$$\begin{aligned}\frac{dSW_{TOA}}{d\ln Aerosol} &= \left.\frac{dSW_{TOA}}{d\ln Aerosol}\right|_{albedo} + \left.\frac{dSW_{TOA}}{d\ln Aerosol}\right|_{CF} \\ &= -SW_{TOA}\times\frac{d\ln N_d}{d\ln Aerosol}\times CF\times[\frac{1}{3}A_{cld}(1-A_{cld})+A_{cld}(1-A_{cld})\times\frac{5}{6}\frac{d\ln LWP}{d\ln N_d}+(A_{cld}-A_{cs})\frac{d\ln CF}{d\ln N_d}]\end{aligned} \quad \textbf{(1)}$$

$$A_{cld} = \frac{0.15\times COD}{2+0.15\times COD} \quad \textbf{(2)}$$

where SW_{TOA} is the net downward shortwave solar radiation at the top of the atmosphere, dSW_{TOA} is the change of net downward shortwave solar radiation at the top of atmosphere (i.e., instantaneous shortwave radiative forcing), and A_{cs} is shortwave broadband ocean surface albedo under clear-sky condition with an average value of 0.02 for the studied region[54]. A_{cld} is the shortwave cloud albedo for liquid clouds, which can be estimated from cloud optical depth (COD, observed by MODIS) using Eq. (2) assuming a solar zenith angle close to zero and an asymmetry factor of 0.85[55]. The A_{cld} average over the studied period and region is about 0.35.

Declarations

Acknowledgments. The machine-learning training is performed using the “Statistics and Machine Learning Toolbox” in MATLAB (version R2019b, MathWorks Inc., Natick, MA, USA). The data storage and processing are performed on high performance computers Stratus, Nimbus and Cumulus, which are supported by the University of Exeter. The views and opinions expressed in this study do not necessarily reflect that of funder. For the purpose of open access, a CC BY public copyright licence is applied to any Author Accepted Manuscript arising from this submission. We would like to thank Chantal Jackson (University of Birmingham) for her contribution to the conceptual figure (Fig. 1b).

Funding. YC is supported by the start-up fund from the University of Birmingham. AP, JH, DP, DG and PF are supported by the UKRI Natural Environment Research Council (NERC) funded ADVANCE project (NE/T006897/1). YW would like to thank the support from the ETH Zurich Foundation (ETH Fellowship project: 2021-HS-332) and Mr. Philippe Sarasin. JH, GJ and FM were also part funded under funding provided by the EU's Horizon 2020 research and innovation programme under the CONSTRAIN grant agreement 820829. JH, PF, GJ and FM are supported by the Joint UK BEIS/Defra Met Office Hadley Centre Climate Programme (GA01101). DG is funded by the National Centre for Atmospheric Science (NCAS), one of the UK NERC’s research centres. NC, LO and SEP are funded by USA NASA programs.

Author contributions. Conceptualization: YC, YW, JH, UL. Methodology: YW, YC, JH. Investigation: YC, JH, YW, UL, FM, GJ, AP, DP, LO, NC, SP, RA. Visualization: YC, YW. Funding acquisition: JH, YW, YC. Writing – original draft: YC, YW, JH. Writing – review & editing: YC, YW, JH, UL, DP, DG, GJ, OL, RA.

Competing Interests. The authors declare no competing interests.

Data and materials availability. The MODIS cloud and aerosol observations from Aqua (MYD08_L3) and Terra (MOD08_L3) used in this study are available at the Atmosphere Archive and Distribution System Distributed Active Archive Center of National Aeronautics and Space Administration (LAADS-DAAC, NASA), https://ladsweb.modaps.eosdis.nasa.gov. Suomi-NPP OMPS SO_2 data is available from NASA Suomi web database: snpp-omps.gesdisc.eosdis.nasa.gov. ERA5 are available from the European Centre for Medium-range Weather Forecast (ECMWF) archive, https://cds.climate.copernicus.eu. GPCP precipitation data is available from NCAR, https://climatedataguide.ucar.edu/climate-data/gpcp-monthly-

global-precipitation-climatology-project. All data needed to evaluate the results in this study are present in the main text and the Supplementary Information.

References

1. IPCC. Climate Change 2021: The Physical Science Basis. Contribution of Working Group I to the Sixth Assessment Report of the Intergovernmental Panel on Climate Change [Masson-Delmotte, V., P. Zhai, A. Pirani, S.L. Connors, C. Péan, S. Berger, N. Caud, Y. Chen, L. Goldfarb, M.I. Gomis, M. Huang, K. Leitzell, E. Lonnoy, J.B.R. Matthews, T.K. Maycock, T. Waterfield, O. Yelekçi, R. Yu, and B. Zhou (eds.)]. *Cambridge University Press, Cambridge, United Kingdom and New York, NY, USA***2391 pp** (2021). https://doi.org:10.1017/9781009157896
2. Watson-Parris, D. & Smith, C. J. Large uncertainty in future warming due to aerosol forcing. *Nature Climate Change* (2022). https://doi.org:10.1038/s41558-022-01516-0
3. Bellouin, N. *et al.* Bounding Global Aerosol Radiative Forcing of Climate Change. *Reviews of Geophysics***58**, e2019RG000660 (2020). https://doi.org:10.1029/2019rg000660
4. Hansen, J. E. *et al.* Global warming in the pipeline. *arXiv preprint arXiv:2212.04474* (2022).
5. Toll, V., Christensen, M., Quaas, J. & Bellouin, N. Weak average liquid-cloud-water response to anthropogenic aerosols. *Nature***572**, 51-55 (2019). https://doi.org:10.1038/s41586-019-1423-9
6. Chen, Y. *et al.* Machine learning reveals climate forcing from aerosols is dominated by increased cloud cover. *Nature Geoscience* (2022). https://doi.org:10.1038/s41561-022-00991-6
7. Latham, J. *et al.* Marine cloud brightening. *Philosophical Transactions of the Royal Society A: Mathematical, Physical and Engineering Sciences***370**, 4217-4262 (2012). https://doi.org:doi:10.1098/rsta.2012.0086
8. Connolly, P. J., McFiggans, G. B., Wood, R. & Tsiamis, A. Factors determining the most efficient spray distribution for marine cloud brightening. *Philosophical Transactions of the Royal Society A: Mathematical, Physical and Engineering Sciences***372**, 20140056 (2014). https://doi.org:doi:10.1098/rsta.2014.0056
9. Tollefson, J. Can artificially altered clouds save the Great Barrier Reef? *Nature***596**, 476-478 (2021). https://doi.org:10.1038/d41586-021-02290-3
10. Twomey, S. Pollution and the planetary albedo. *Atmospheric Environment***8**, 1251-1256 (1974). https://doi.org:https://doi.org/10.1016/0004-6981(74)90004-3
11. Albrecht, B. A. Aerosols, Cloud Microphysics, and Fractional Cloudiness. *Science***245**, 1227-1230 (1989). https://doi.org:10.1126/science.245.4923.1227
12. Ackerman, A. S., Kirkpatrick, M. P., Stevens, D. E. & Toon, O. B. The impact of humidity above stratiform clouds on indirect aerosol climate forcing. *Nature***432**, 1014-1017 (2004). https://doi.org:10.1038/nature03174
13. Ghan, S. *et al.* Challenges in constraining anthropogenic aerosol effects on cloud radiative forcing using present-day spatiotemporal variability. *Proceedings of the National Academy of Sciences***113**,

5804-5811 (2016). https://doi.org:10.1073/pnas.1514036113

14. Stjern, C. W. *et al.* Response to marine cloud brightening in a multi-model ensemble. *Atmos. Chem. Phys.* **18**, 621-634 (2018). https://doi.org:10.5194/acp-18-621-2018
15. Seinfeld, J. H. *et al.* Improving our fundamental understanding of the role of aerosol–cloud interactions in the climate system. *Proceedings of the National Academy of Sciences* **113**, 5781-5790 (2016). https://doi.org:10.1073/pnas.1514043113
16. Manshausen, P., Watson-Parris, D., Christensen, M. W., Jalkanen, J.-P. & Stier, P. Invisible ship tracks show large cloud sensitivity to aerosol. *Nature* **610**, 101-106 (2022). https://doi.org:10.1038/s41586-022-05122-0
17. Rosenfeld, D. *et al.* Aerosol-driven droplet concentrations dominate coverage and water of oceanic low-level clouds. *Science* **363**, eaav0566 (2019). https://doi.org:10.1126/science.aav0566
18. Malavelle, F. F. *et al.* Strong constraints on aerosol–cloud interactions from volcanic eruptions. *Nature* **546**, 485-491 (2017). https://doi.org:10.1038/nature22974
19. Glassmeier, F. *et al.* Aerosol-cloud-climate cooling overestimated by ship-track data. *Science* **371**, 485-489 (2021). https://doi.org:10.1126/science.abd3980
20. Quaas, J. *et al.* Constraining the Twomey effect from satellite observations: issues and perspectives. *Atmos. Chem. Phys.* **20**, 15079-15099 (2020). https://doi.org:10.5194/acp-20-15079-2020
21. Slingo, A. Sensitivity of the Earth's radiation budget to changes in low clouds. *Nature* **343**, 49-51 (1990). https://doi.org:10.1038/343049a0
22. Breen, K. H., Barahona, D., Yuan, T., Bian, H. & James, S. C. Effect of volcanic emissions on clouds during the 2008 and 2018 Kilauea degassing events. *Atmos. Chem. Phys.* **21**, 7749-7771 (2021). https://doi.org:10.5194/acp-21-7749-2021
23. Kravitz, B. *et al.* The Geoengineering Model Intercomparison Project Phase 6 (GeoMIP6): simulation design and preliminary results. *Geosci. Model Dev.* **8**, 3379-3392 (2015). https://doi.org:10.5194/gmd-8-3379-2015
24. Andreae, M. O., Jones, C. D. & Cox, P. M. Strong present-day aerosol cooling implies a hot future. *Nature* **435**, 1187-1190 (2005).
25. Wall, C. J. *et al.* Assessing effective radiative forcing from aerosol–cloud interactions over the global ocean. *Proceedings of the National Academy of Sciences* **119**, e2210481119 (2022). https://doi.org:doi:10.1073/pnas.2210481119
26. Robock, A., Jerch, K. & Bunzl, M. 20 reasons why geoengineering may be a bad idea. *Bulletin of the Atomic Scientists* **64**, 14-59 (2008). https://doi.org:10.1080/00963402.2008.11461140
27. Toll, V., Christensen, M., Gassó, S. & Bellouin, N. Volcano and Ship Tracks Indicate Excessive Aerosol-Induced Cloud Water Increases in a Climate Model. *Geophysical Research Letters* **44**, 12,492-412,500 (2017). https://doi.org:10.1002/2017gl075280
28. Wood, R. & Bretherton, C. S. On the Relationship between Stratiform Low Cloud Cover and Lower-Tropospheric Stability. *Journal of Climate* **19**, 6425-6432 (2006).

https://doi.org:https://doi.org/10.1175/JCLI3988.1

29. Christensen, M. W., Jones, W. K. & Stier, P. Aerosols enhance cloud lifetime and brightness along the stratus-to-cumulus transition. *Proceedings of the National Academy of Sciences***117**, 17591-17598 (2020). https://doi.org:10.1073/pnas.1921231117
30. Gryspeerdt, E. *et al.* Constraining the aerosol influence on cloud liquid water path. *Atmos. Chem. Phys.***19**, 5331-5347 (2019). https://doi.org:10.5194/acp-19-5331-2019
31. Stevens, B. & Feingold, G. Untangling aerosol effects on clouds and precipitation in a buffered system. *Nature***461**, 607-613 (2009). https://doi.org:10.1038/nature08281
32. Quaas, J. Evaluating the “critical relative humidity” as a measure of subgrid-scale variability of humidity in general circulation model cloud cover parameterizations using satellite data. *Journal of Geophysical Research: Atmospheres***117** (2012). https://doi.org:https://doi.org/10.1029/2012JD017495
33. Arola, A. *et al.* Aerosol effects on clouds are concealed by natural cloud heterogeneity and satellite retrieval errors. *Nature Communications***13**, 7357 (2022). https://doi.org:10.1038/s41467-022-34948-5
34. Grosvenor, D. P. *et al.* Remote Sensing of Droplet Number Concentration in Warm Clouds: A Review of the Current State of Knowledge and Perspectives. *Reviews of Geophysics***56**, 409-453 (2018). https://doi.org:https://doi.org/10.1029/2017RG000593
35. Grosvenor, D. P. & Wood, R. The effect of solar zenith angle on MODIS cloud optical and microphysical retrievals within marine liquid water clouds. *Atmos. Chem. Phys.***14**, 7291-7321 (2014). https://doi.org:10.5194/acp-14-7291-2014
36. Yuan, T. *et al.* Global reduction in ship-tracks from sulfur regulations for shipping fuel. *Science Advances***8**, eabn7988 (2022). https://doi.org:doi:10.1126/sciadv.abn7988
37. Gryspeerdt, E., Quaas, J. & Bellouin, N. Constraining the aerosol influence on cloud fraction. *Journal of Geophysical Research: Atmospheres***121**, 3566-3583 (2016). https://doi.org:https://doi.org/10.1002/2015JD023744
38. Quaas, J. *et al.* Robust evidence for reversal in the aerosol effective climate forcing trend. *Atmos. Chem. Phys. Discuss.***2022**, 1-25 (2022). https://doi.org:10.5194/acp-2022-295
39. Misumi, R. *et al.* Classification of aerosol-cloud interaction regimes over Tokyo. *Atmospheric Research***272**, 106150 (2022). https://doi.org:https://doi.org/10.1016/j.atmosres.2022.106150
40. Muench, S. & Lohmann, U. Developing a Cloud Scheme With Prognostic Cloud Fraction and Two Moment Microphysics for ECHAM-HAM. *Journal of Advances in Modeling Earth Systems***12**, e2019MS001824 (2020). https://doi.org:https://doi.org/10.1029/2019MS001824
41. Tompkins, A. M. A Prognostic Parameterization for the Subgrid-Scale Variability of Water Vapor and Clouds in Large-Scale Models and Its Use to Diagnose Cloud Cover. *Journal of the Atmospheric Sciences***59**, 1917-1942 (2002). https://doi.org:https://doi.org/10.1175/1520-0469(2002)059<1917:APPFTS>2.0.CO;2

References for Methods and Supplementary Information:

42. Yuan, T., Remer, L. A. & Yu, H. Microphysical, macrophysical and radiative signatures of volcanic aerosols in trade wind cumulus observed by the A-Train. *Atmos. Chem. Phys.***11**, 7119-7132 (2011). https://doi.org:10.5194/acp-11-7119-2011

43. Hamilton, D. S. *et al.* Occurrence of pristine aerosol environments on a polluted planet. *Proceedings of the National Academy of Sciences***111**, 18466-18471 (2014). https://doi.org:doi:10.1073/pnas.1415440111

44. Elias, T., Kern, C., Horton, K. A., Sutton, A. J. & Garbeil, H. Measuring SO2 Emission Rates at Kīlauea Volcano, Hawaii, Using an Array of Upward-Looking UV Spectrometers, 2014–2017. *Frontiers in Earth Science***6** (2018). https://doi.org:10.3389/feart.2018.00214

45. Neal, C. A. *et al.* The 2018 rift eruption and summit collapse of Kīlauea Volcano. *Science***363**, 367-374 (2019). https://doi.org:doi:10.1126/science.aav7046

46. Huffman, G. J. *et al.* The Global Precipitation Climatology Project (GPCP) Combined Precipitation Dataset. *Bulletin of the American Meteorological Society***78**, 5-20 (1997). https://doi.org:10.1175/1520-0477(1997)078<0005:tgpcpg>2.0.co;2

47. Hersbach, H. *et al.* The ERA5 global reanalysis. *Quarterly Journal of the Royal Meteorological Society***146**, 1999-2049 (2020). https://doi.org:https://doi.org/10.1002/qj.3803

48. Hubanks, P., Platnick, A. S., King, M. & Ridgway, B. MODIS Atmosphere L3 Gridded Product Algorithm Theoretical Basis Document (ATBD) & Users Guide. *available from: https://icdc.cen.uni-hamburg.de/fileadmin/user_upload/icdc_Dokumente/MODIS/MODIS_Collection6_AtmosphereL3_GriddedProduct_ATBDandUsersGuide_v4.1_Sep22_2015.pdf* (2019).

49. Quaas, J., Boucher, O. & Lohmann, U. Constraining the total aerosol indirect effect in the LMDZ and ECHAM4 GCMs using MODIS satellite data. *Atmos. Chem. Phys.***6**, 947-955 (2006). https://doi.org:10.5194/acp-6-947-2006

50. Quaas, J., Boucher, O., Bellouin, N. & Kinne, S. Satellite-based estimate of the direct and indirect aerosol climate forcing. *Journal of Geophysical Research: Atmospheres***113** (2008). https://doi.org:https://doi.org/10.1029/2007JD008962

51. Bastos, L. S. & O'Hagan, A. Diagnostics for Gaussian Process Emulators. *Technometrics***51**, 425-438 (2009). https://doi.org:10.1198/TECH.2009.08019

52. Loeb, N. G. *et al.* Clouds and the Earth's Radiant Energy System (CERES) Energy Balanced and Filled (EBAF) Top-of-Atmosphere (TOA) Edition-4.0 Data Product. *Journal of Climate***31**, 895-918 (2018). https://doi.org:10.1175/jcli-d-17-0208.1

53. Ackerman, A. S. *et al.* Effects of Aerosols on Cloud Albedo: Evaluation of Twomey's Parameterization of Cloud Susceptibility Using Measurements of Ship Tracks. *Journal of the Atmospheric Sciences***57**, 2684-2695 (2000). https://doi.org:10.1175/1520-0469(2000)057<2684:eoaoca>2.0.co;2

54. Jin, Z., Charlock, T. P., Smith Jr., W. L. & Rutledge, K. A parameterization of ocean surface albedo. *Geophysical Research Letters***31** (2004). https://doi.org:https://doi.org/10.1029/2004GL021180

55. Feingold, G. *et al.* Analysis of albedo versus cloud fraction relationships in liquid water clouds using heuristic models and large eddy simulation. *Journal of Geophysical Research: Atmospheres***122**,

7086-7102 (2017). https://doi.org:https://doi.org/10.1002/2017JD026467

56. IPCC. Guidance Note for Lead Authors of the IPCC Fifth Assessment Report on Consistent Treatment of Uncertainties. https://www.ipcc.ch/site/assets/uploads/2017/2008/AR2015_Uncertainty_Guidance_Note.pdf (2010).
57. Cho, N., Tan, J. & Oreopoulos, L. Classifying Planetary Cloudiness with an Updated Set of MODIS Cloud Regimes. *Journal of Applied Meteorology and Climatology* **60**, 981-997 (2021). https://doi.org:10.1175/jamc-d-20-0247.1

Figures

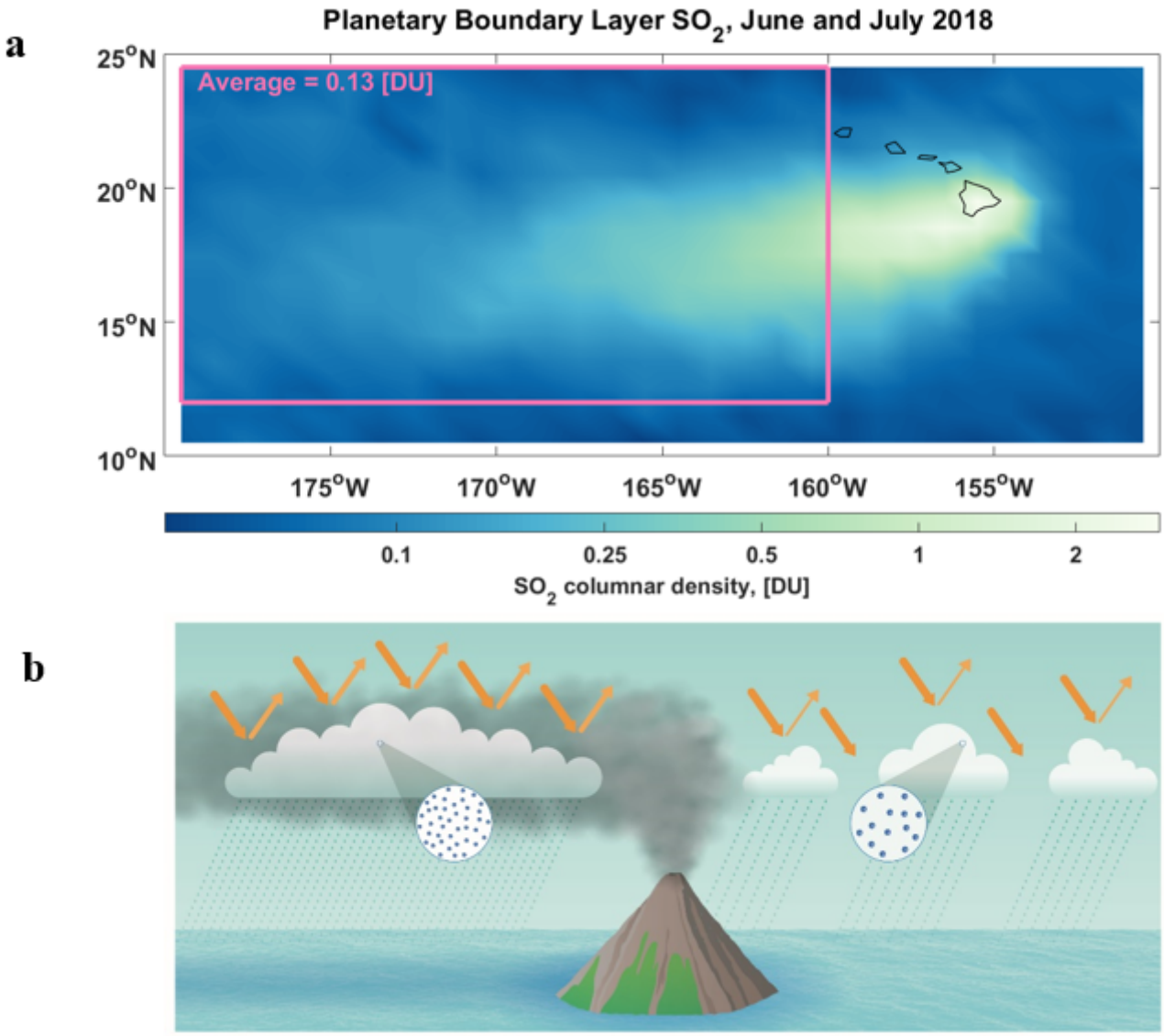

Figure 1

Kilauea volcanic plume. (a) SO2 plume observed by satellite in June and July 2018. The color shows planetary boundary layer SO_2 plume observed by Ozone Mapping and Profiler Suite (OMPS) Sensor on the Suomi-NPP satellite, launched in October 2011. Here we aggregate the daily level-2 product of boundary layer column SO_2 (horizontal resolution of about 50 km) to a 2-month average. The studied region is marked by pink box, where plume dispersal was both efficient and sufficiently displaced from the Hawaii Islands to avoid orographic effects. **(b)** Conceptual picture of volcanic aerosol plume interacts with shallow convective marine clouds, leading to increase of cloud cover, precipitation and more reflected solar radiation back to space.

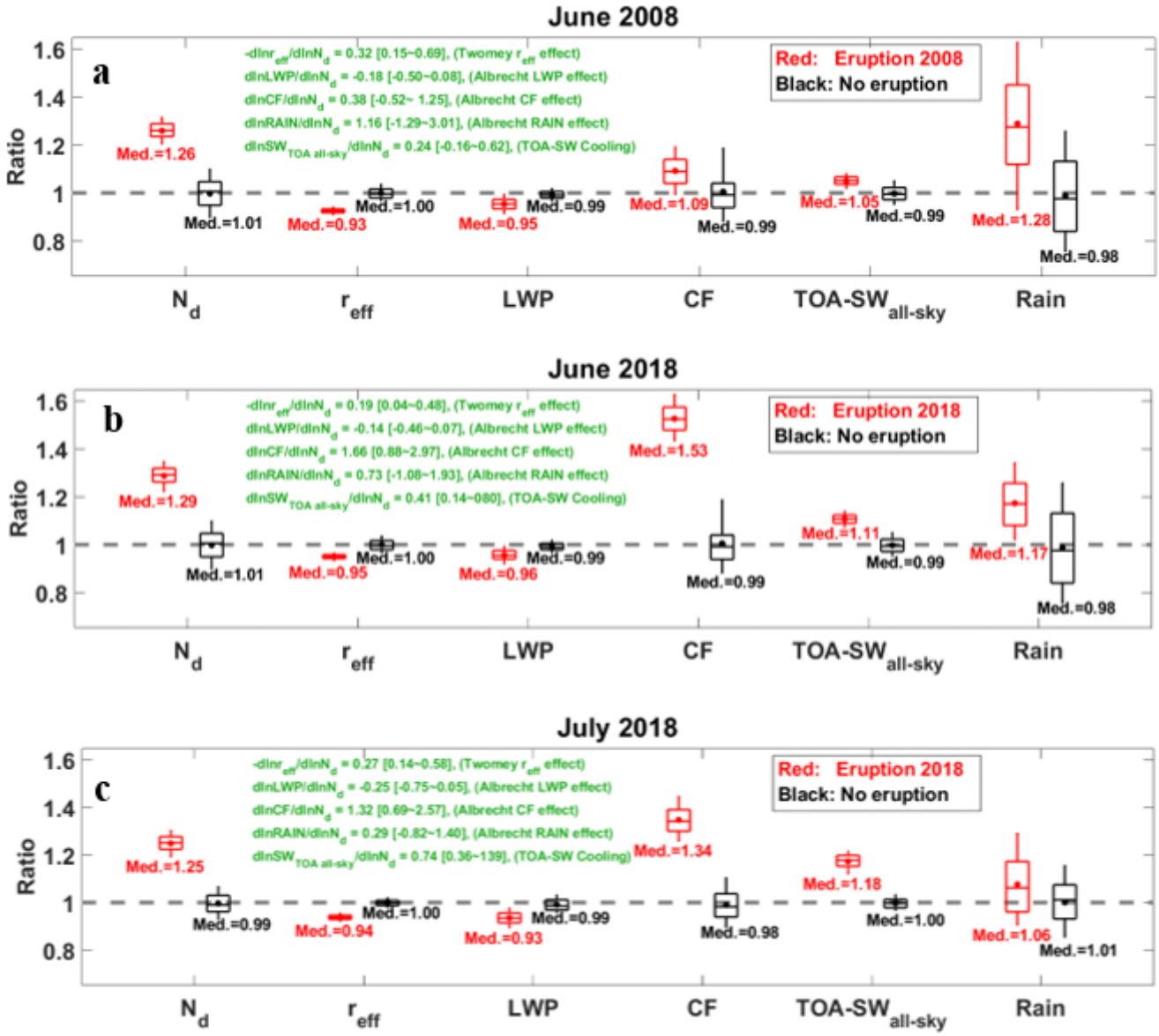

Figure 2

Aerosol fingerprints on clouds from natural experiments. Panel **(a)** June 2008, **(b)** June 2018, and **(c)** July 2018. The aerosol-induced responses of clouds are shown in red, as ratios between observations and machine-learning surrogates; non-perturbed baselines of normal conditions are shown in black. The

boxplots show 10th, 25th, median (Med.), 75th and 90th percentiles with the average indicated by a dot. The uncertainty is estimated by a bootstrapping Monte Carlo method (see Methods), with black boxes showing the validation of machine-learning surrogate against observations under normal conditions. The susceptibilities of r_{eff}, LWP and CF to changes in N_d are show in green, median [90% confidence interval]. Area (in units of km^2) weighted averaging is used to calculate average cloud properties over the geographical region (the red box in Fig. 1a), in order to estimate an unbiased large-scale response. All the ACI signals, i.e. the differences between the red and black boxes, pass the Mann-Whitney-Wilcoxom test with significance > 95% (p-value < 0.05).

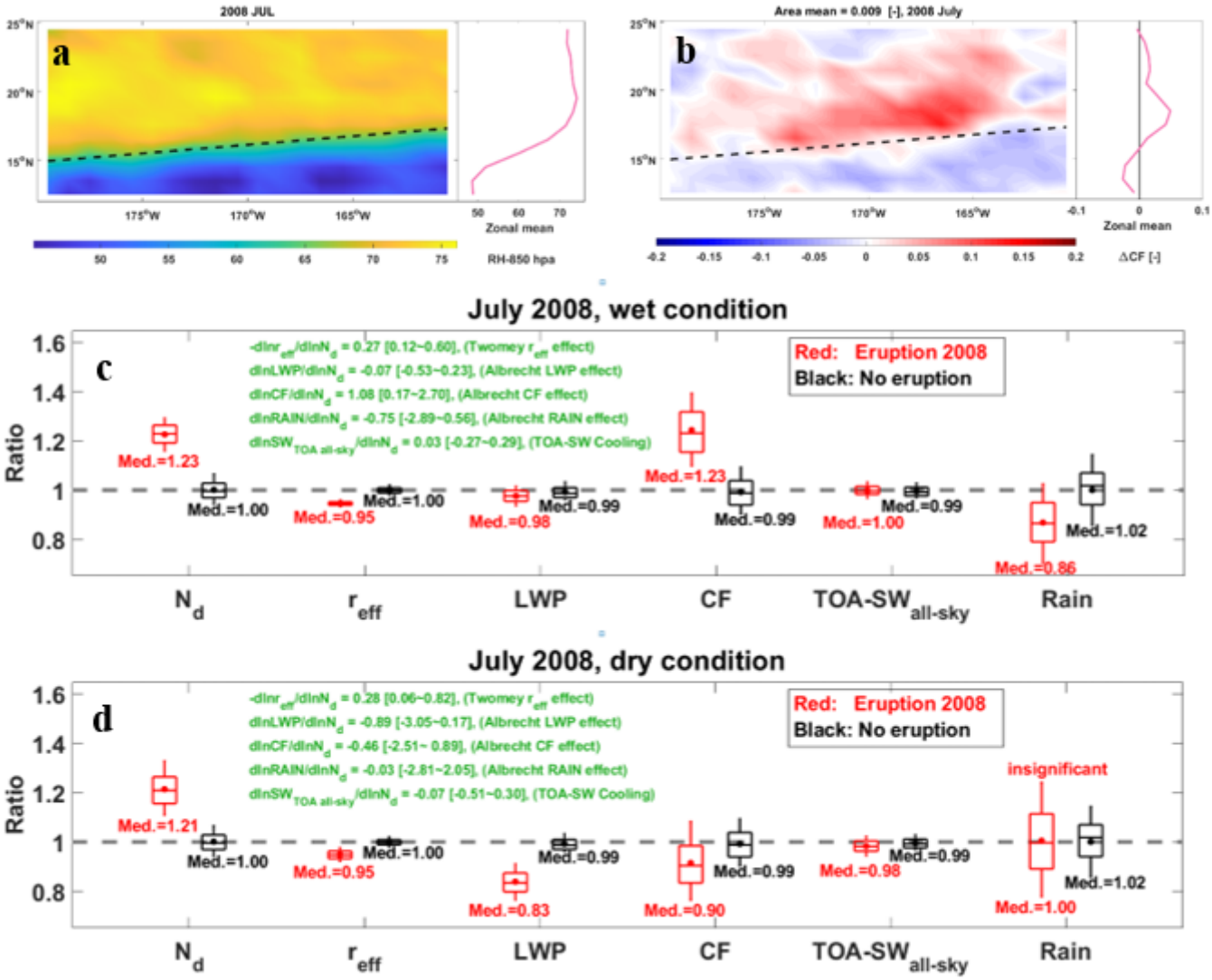

Figure 3

Aerosol fingerprints on clouds. Natural experiment of July 2008 with humid condition in the northern part and very dry conditions in the southern part. Panel **(a)** shows the distribution of RH at 850 hPa, **(b)**the response of cloud fraction to aerosol perturbations, **(c)** ACI manifestations for wet conditions, and **(d)** ACI

manifestations for dry conditions. All the fingerprint signals pass the Mann-Whitney-Wilcoxom test with significance > 95%, unless marked as “insignificant”.

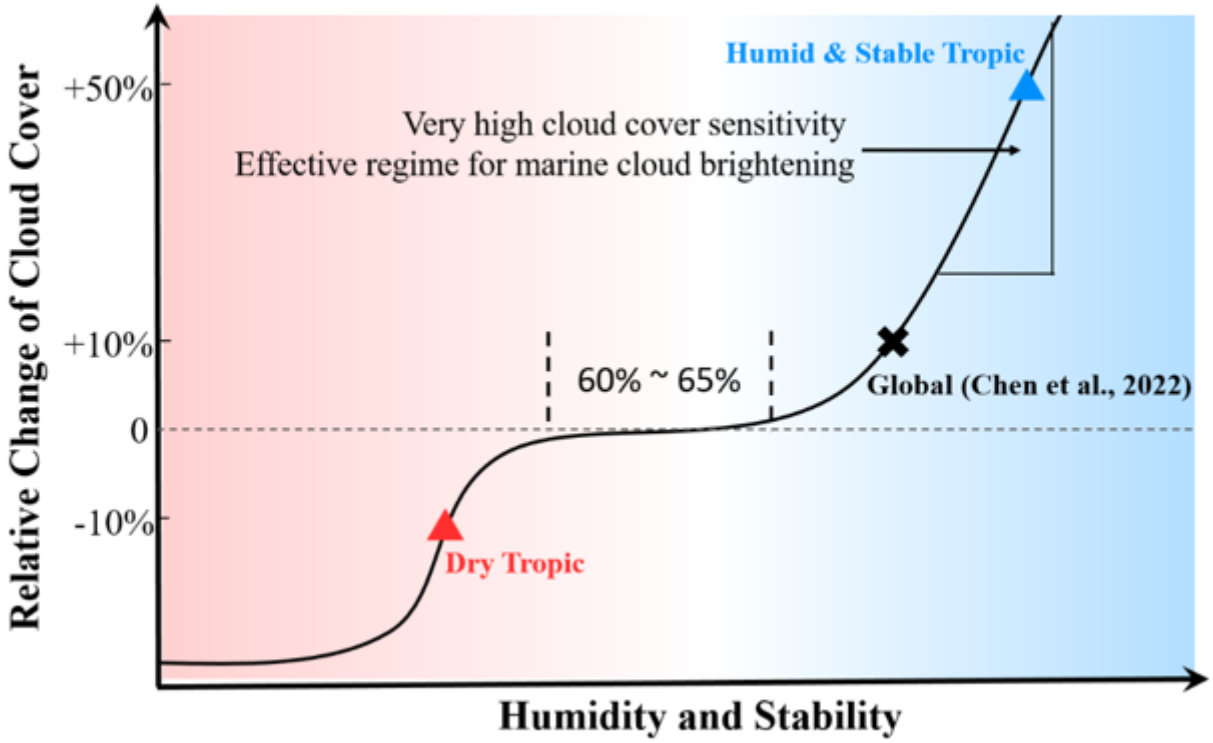

Figure 4

Conceptual model of cloud cover’s response to aerosol perturbation. The responses depend on meteorology conditions and cloud regimes. The Holuhraun study in Chen et al. (2022) represents a more generalized analogy for the global cloud regime spectrum, while this study represents a cloud regime spectrum for tropical marine clouds that could potentially be used for marine cloud brightening; they are all marked in the figure. The effective meteorology regime for MCB is highlighted in blue.

Supplementary Files

This is a list of supplementary files associated with this preprint. Click to download.

- ChensupplementNatureGeosci.docx
- ExtendedDataFig.docx